THE JOURNAL OF BIOLOGICAL CHEMISTRY VOL. 286, NO. 29, pp. 25922–25934, July 22, 2011

Normal Fur Development and Sebum Production Depends on Fatty Acid 2-Hydroxylase Expression in Sebaceous Glands*

Received for publication, February 16, 2011, and in revised form, May 18, 2011 Published, JBC Papers in Press, May 31, 2011, DOI 10.1074/jbc.M111.231977

Helena Maier[‡], Marion Meixner[‡], Dieter Hartmann[§], Roger Sandhoff[¶], Lihua Wang-Eckhardt[‡], Inge Zöller[‡], Volkmar Gieselmann[‡], and Matthias Eckhardt[‡1]

From the [‡]Institute of Biochemistry and Molecular Biology and [§]Institute of Anatomy, University of Bonn, D-53115 Bonn and the [¶]German Cancer Research Center, 69120 Heidelberg, Germany

2-Hydroxylated fatty acid (HFA)-containing sphingolipids are abundant in mammalian skin and are believed to play a role in the formation of the epidermal barrier. Fatty acid 2-hydroxylase (FA2H), required for the synthesis of 2-hydroxylated sphingolipids in various organs, is highly expressed in skin, and previous *in vitro* studies demonstrated its role in the synthesis of HFA sphingolipids in human keratinocytes. Unexpectedly, however, mice deficient in FA2H did not show significant changes in their epidermal HFA sphingolipids. Expression of FA2H in murine skin was restricted to the sebaceous glands, where it was required for synthesis of 2-hydroxylated glucosylceramide and a fraction of type II wax diesters. Absence of FA2H resulted in hyperproliferation of sebocytes and enlarged sebaceous glands during hair follicle morphogenesis and anagen (active growth phase) in adult mice. This was accompanied by a significant up-regulation of the epidermal growth factor receptor ligand epigen in sebocytes. Loss of FA2H significantly altered the composition and physicochemical properties of sebum, which often blocked the hair canal, apparently causing a delay in the hair fiber exit. Furthermore, mice lacking FA2H displayed a cycling alopecia with hair loss in telogen. These results underline the importance of the sebaceous glands and suggest a role of specific sebaceous gland or sebum lipids, synthesized by FA2H, in the hair follicle homeostasis.

Hair in mammals is formed by the hair follicle, which undergoes repeated cycles of growth (anagen), regression (catagen), and resting phases (telogen) (for review see Ref. 1 and references therein). During anagen, a new hair shaft is generated, followed by shedding of the old hair, possibly by an actively induced process called exogen (2, 3). Regeneration of the hair follicle in anagen depends on newly generated proliferating matrix cells at the base of the follicle, which are derived from stem cells in the bulge region, located in close proximity to the sebaceous gland (SG).[2] Various genetic defects can affect normal hair cycling, causing excessive hair growth or abnormal hair loss (see Ref. 1 and references therein).

The mammalian skin produces large amounts of different and in part skin-specific lipids. For example, ω-hydroxylated ceramides covalently bound to proteins in the cornified envelope are essential components of the water barrier of the skin (4). The major fraction of the noncovalently bound skin surface lipids is derived from the sebum produced by SG and released by holocrine secretion (5, 6). In general, sebum is deposited on the hair inside the follicle and is brought up to the surface of the skin along the hair shaft. Sebum lubricates and protects the hair and skin and prevents drying and irritation of membranes. Sebum lipids possibly play a role in waterproofing, and antibacterial sebum lipids may inhibit infections of the skin (5). Significant species-specific differences in the sebum composition exist, but their functional relevance is largely unknown (7). Although the production of sebum is the only established role of SG, several studies suggest that they may also play a role in hair follicle homeostasis (8–10).

Mammalian epidermis contains large amounts of ceramide, glucosylceramide, and sphingomyelin synthesized by differentiating keratinocytes (11). Most ceramides of the stratum corneum derive from glucosylceramide and sphingomyelin and are liberated from these precursors by extracellular hydrolysis. The transient "conversion" of free ceramides into other sphingolipids enables keratinocytes to produce large amounts of ceramides without increasing intracellular free ceramide concentration, which otherwise could affect various signaling pathways (11). In contrast to the established role of ceramide ω-hydroxylation (see above), much less is known about the function of other hydroxyl modifications found in skin sphingolipids, like 2-hydroxylation of the acyl residues and 4-hydroxylation of the sphingoid base.

Mammalian skin contains relatively large amounts of 2-hydroxylated sphingolipids. In line with this, the only known enzyme catalyzing the 2-hydroxylation of unbranched fatty acids, fatty acid 2-hydroxylase (FA2H) (12–14), is highly expressed in murine skin (13). Furthermore, differentiation-dependent up-regulation of *Fa2h* has been observed in human keratinocytes (15), suggesting that FA2H is responsible for synthesis of 2-hydroxylated sphingolipids in keratinocytes of mammalian skin. To further explore the role of 2-hydroxylated sphingolipids, we have generated FA2H-deficient mice (16). These mice lack all 2-hydroxylated sphingolipids in the central and peripheral nervous system. Nevertheless, normal compact myelin was formed in these mice. However, aged mice develop

* This work was supported by the Deutsche Forschungsgemeinschaft Grant SFB645 from the University of Bonn.

[1] To whom correspondence should be addressed: Institute of Biochemistry and Molecular Biology, University of Bonn, Nussallee 11, 53115 Bonn, Germany. Tel.: 49-228-73-4735; Fax: 49-228-73-2416; E-mail: eckhardt@uni-bonn.de.

[2] The abbreviations used are: SG, sebaceous gland; Epgn, epigen; FA2H, fatty acid 2-hydroxylase; GlcCer, glucosylceramide; HFA, 2-hydroxylated fatty acid; HFA-GlcCer, 2-hydroxylated glucosylceramide; ORS, outer root sheath; PPARγ, peroxisome proliferator-activated receptor-γ.

a late onset axon and myelin sheath degeneration (16). Unexpectedly, we found that synthesis of most 2-hydroxylated sphingolipids in murine skin does not depend on *Fa2h* expression. In murine skin, *Fa2h* is only expressed in SG and not in keratinocytes. Absence of FA2H affected synthesis of 2-hydroxylated glucosylceramide and wax diesters in the SG and caused a delay in fur emergence, sebocyte hyperproliferation, and cyclic alopecia.

EXPERIMENTAL PROCEDURES

FA2H-deficient Mice—FA2H-deficient mice were generated as described previously (16). Genotyping was done by PCR on genomic mouse tail DNA using the oligonucleotides 5′-ATTCGCAGCGCATCGCCTTCTATC-3′, 5′-GTGCTGTACCTCAGCTGGTC-3′, and 5′-GCTCTTCTTCAAGAGCCATCC-3′ as primers, which amplified a 1045-bp fragment from the wild-type and a 685-bp fragment from the targeted allele. All animal experiments were approved by and carried out with permission from the Landesamt für Natur, Umwelt und Verbraucherschutz, Nordrhein-Westfalen, Germany.

FA2H Antiserum—An antiserum directed against mouse FA2H was generated by immunization of rabbits with the peptide CELRADPQDPTENGA linked to keyhole limpet hemocyanin via the amino-terminal cysteine residue. The peptide sequence corresponds to amino acids 84–97 of the FA2H protein. The monospecific IgG fraction was isolated by affinity chromatography. Because FA2H-deficient mice have an insertion of a *lacZ* reporter gene in exon 3, mice express a fusion protein of the amino-terminal cytochrome b_5 domain with β-galactosidase, which is also recognized by the FA2H antiserum. Specificity of the antiserum was tested by immunofluorescence and Western blot analysis using CHO cells transfected with an *Fa2h* expression plasmid (data not shown).

Northern Blot Analysis—Total RNA of murine skin was isolated using TRIzol (Invitrogen) as described by the manufacturer. Total RNA (20 μg/lane) was separated in 1 M formaldehyde, 1% agarose gels and transferred onto Hybond-N^+ nylon membranes (Amersham Biosciences). A 568-bp fragment of the Fa2h cDNA (corresponding to exon 3 and 4) was used to synthesize a ^{32}P-labeled probe by random priming using [α-^{32}P]dCTP and Megaprime DNA labeling kit (Amersham Biosciences), following the instructions of the manufacturer. A β-actin probe (Stratagene, La Jolla, CA) was used to control for equal loading. Hybridization was performed using standard procedures (17). Radioactivity was detected by autoradiography on x-ray films.

In Situ Hybridization—Digoxigenin-labeled cRNA probes were transcribed from FA2H cDNA as described previously (13). Hybridization of digoxigenin-labeled cRNA probes to skin paraffin sections was done as described previously (18). Briefly, sections were hybridized overnight at 70 °C in 50% formamide, 1% Denhardt' solution, 0.2% SDS, 0.25 mg/ml salmon sperm DNA, 0.3 M NaCl, 10 mM PIPES, and 10 mM EDTA. Sections were washed twice with 2× SSC at 60 °C for 5 and 30 min and once with 0.1× SSC for 45 min at 70 °C. Hybridized sections were equilibrated in maleic acid buffer (100 mM maleic acid, 150 mM NaCl, pH 7.5) and incubated in maleic acid buffer containing 2% blocking reagent (Roche Diagnostics) for 1 h at room temperature. Bound RNA probes were detected using alkaline phosphatase-conjugated anti-digoxigenin Ig (Roche Diagnostics) at a dilution of 1:5,000 in maleic acid buffer containing 2% blocking reagent (Roche Diagnostics) at 4 °C overnight in a humid chamber. Sections were washed with alkaline phosphatase buffer (100 mM Tris-HCl, 100 mM NaCl, 50 mM $MgCl_2$, pH 9.5) and stained using 0.33 mg/ml nitro blue tetrazolium and 0.16 mg/ml 5-bromo-4-chloro-3-indolyl phosphate in alkaline phosphatase buffer containing 2 mM levamisole to block endogenous alkaline phosphatase activity.

Histological Analysis and Immunofluorescence—Back skin samples were directly frozen in OCT Tissue-TeK as described by Paus *et al.* (19). Sections (8–10 μm) were cut in a cryostat and postfixed in 4% paraformaldehyde (PFA) in phosphate-buffered saline (PBS). Alternatively, skin samples were fixed overnight with 4% PFA in PBS at 4 °C and embedded in paraffin. Sections of 6 μm were placed on Superfrost Plus slides (Menzel-Gläser, Braunschweig, Germany) and dried overnight. After deparaffination in xylene and rehydration in an ethanol series, sections were either stained with hematoxylin and eosin (H&E staining) for histology or processed for 15 min in 10 mM sodium citrate buffer, pH 6.0, in a microwave oven for antigen retrieval. Sections were slowly cooled down to room temperature, rinsed in Tris-buffered saline (TBS), and permeabilized with 0.5% Triton X-100 in TBS for 10 min. After blocking with 6% bovine serum albumin (BSA) in TBS for 1 h, the sections were incubated with anti-Ki-67 antibody (DAKO Deutschland GmbH, Hamburg, Germany) (1:25) and the above-mentioned FA2H antiserum (1:800) or anti-CD34 antibody (Hycult® Biotech, Beutelsbach, Germany) (1:25) and the above-mentioned FA2H antiserum (1:800) overnight at 4 °C. After washing with TBS, Cy3-conjugated goat anti-rabbit (1:500; The Jackson Laboratory) and Alexa 488-conjugated goat anti-rat (1:200; Molecular Probes, Eugene, OR) were used to detect primary antibodies. All antibodies were diluted in 1% BSA in TBS. Nuclei were stained with 4′,6-diamidino-2-phenylindole (DAPI) (Sigma), and the sections were embedded in polyvinyl alcohol mounting medium with 1,4-diazabicyclo[2.2.2]octane (Sigma). Images were captured with an Axiovert 100M fluorescence microscope (Carl Zeiss, Jena, Germany) and analyzed with the Axiovision 4.5 program. SG size was quantified by morphometric measurements with the Axiovision 4.5 program.

BrdU Labeling and Immunohistochemistry—Mice were injected (intraperitoneally) with 10 μl of BrdU labeling reagent (100 mg/ml; BioGenex, San Ramon, CA)/g body weight, 2.5 h before they were sacrificed. Dorsal skin samples were fixed, embedded, and sectioned as described above. After deparaffination, the sections were placed in 2 N HCl for 30 min at 37 °C and subsequently rinsed thoroughly in PBS. This was followed by a 30-min treatment with 0.1% trypsin (Invitrogen) in PBS at 37 °C. After rinsing in PBS, the sections were covered with the monoclonal anti-BrdU antibody IIB5 (BioGenex) overnight at 4 °C. For detection with horseradish peroxidase-conjugated secondary antibodies, the Super Sensitive™ Link-Label IHC detection system (BioGenex) was used with 3,3′-diaminobenzidine as substrate. Sections were counterstained with hematoxylin for 30 s, dehydrated, and embedded in polyvinyl alcohol mounting medium with 1,4-diazabicyclo[2.2.2]octane (Sigma).

TABLE 1
Sequences of oligonucleotides used for real-time PCR

Target gene	Forward primer	Reverse primer
Ubiquitin C (*UbC*)	AGGCAAGACCATCACCTTGGACG	CCATCACACCCAAGAACAAGCACA
Heparin-binding EGF-like growth factor (*Hb-egf*)	TATGACCACACTACAGTCTTG	TCATAACCTCCTCTCCTGTG
Epithelial mitogen (*Epgn*)	ATTCCACCATGAGCTGAAGC	ATCCACAGCATACGAAGTTAG
Fatty acid 2-hydroxylase (*Fa2h*) exons 1/2	CTGGCTGGAGCAGTACTATG	GTCTGTCTTCTGAGTCTCTG
Fatty acid 2-hydroxylase (*Fa2h*) exons 5/6	AGCCATTACCTCATCATGTTG	TAGAAGAAGGCAATCACTAGG
Melanocortin 5 receptor (*Mc5r*)	CGTGAAGAATCATGCTTACCT	GGAGTTCATTGCTGGAAGAG
Neuregulin 4 (*Nrg4*)	CAGGCACAGGTCATTTTGC	AAGTAGGCAATGTCTTAGAAAC
Stearoyl-coenzyme A desaturase 1 (*Scd1*)	CTACGACAAGAACATTCAATCC	TACTCACTGGCAGAGTAGTC
Stearoyl-coenzyme A desaturase 2 (*Scd2*)	ACGACAAGAACATTAGCTCTC	TACTCACTGGCAGAGTAGTC
Stearoyl-coenzyme A desaturase 3 (*Scd3*)	GGACATGTCTGACCTGAAAG	GCAGGATGAAGCACATCAGC
Peroxisome proliferator activated receptor γ (*Ppar*γ)	CAATGCACTGGAATTAGATGAC	CTTCACGTTCAGCAAGCCTG

Microarray Hybridization—RNA was prepared from back skin of postnatal day 10 wild-type ($n = 2$), $Fa2h^{+/-}$ ($n = 3$), and $Fa2h^{-/-}$ ($n = 3$) mice using TRIzol, according to the manufacturer's instructions. Total RNA was further purified using RNeasy mini-columns (Qiagen, Hilden, Germany). cDNA was synthesized from 5 μg of total RNA using T7-oligo(dT) primers. Synthesis of biotin-labeled cRNA and cRNA fragmentation was done following the protocols from Affymetrix (Santa Clara, CA). Ten μg of fragmented cRNA were hybridized to Affymetrix GeneChip mouse genome 430 2.0 arrays following the manufacturer's instructions. Microarray data were analyzed with ArrayAssist (Agilent Technologies, Waldbronn, Germany) using the GC-Robust Multiarray Averaging method for normalization.

Real Time RT-PCR—Skin total RNA was isolated using TRIzol (Invitrogen), following the instructions of the manufacturer. cDNA was synthesized from skin total RNA (5 μg) using Superscript II reverse transcriptase (Invitrogen) and oligo(dT) primers. Real time PCR was done using a Bio-Rad i-cycler (Bio-Rad) and SYBR Green ReadyMix (Sigma). Data were analyzed by the $2^{-\Delta Ct}$ method, using ubiquitin C as the reference. Data are shown as means ± S.E. Data were tested for significance using two-tailed t test with a significance level of $p < 0.05$. All PCRs were done in duplicate, and at least three independent experiments using RNA preparations from three mice per genotype and age were performed. The primer sequences used to amplify specific target cDNAs are listed in Table 1.

Lipid Analysis by TLC—Epidermis was isolated by incubating back skin samples with dispase II (0.8 units/ml; Roche Diagnostics) at 4 °C for 16–18 h. Alternatively, epidermis was separated from dermis by 16–18 h of incubation on 1% trypsin in Hepes buffer, pH 7.4. Epidermis was removed and lyophilized. Lipids were isolated from dried epidermis, total skin, or auricles as described previously (20). Lipids were separated by thin layer chromatography (TLC) on Silica Gel 60 HPTLC plates (Merck) using the solvent system chloroform/methanol/acetic acid (190:9:1, v/v) for ceramides or chloroform/methanol/water (65:25:4, v/v) for hexosylceramides. Surface lipids, which are mostly derived from SG (7), were extracted by dipping mice into 20–30 ml of acetone. The acetone extract was filtered through glass wool and dried under nitrogen. Total surface lipids were analyzed by TLC using the solvent system *n*-hexane/toluene (1:1, v/v) or chloroform/methanol/acetic acid (190:9:1, v/v). The following standards were used: cholesterol, oleyl oleate, triglycerides, and cholesterol ester (all from Sigma). Standard lipids were applied onto the same TLC plate as the samples and used to generate a standard curve. After scanning, lipids were quantified by densitometry with the Advanced Image data analyzer software (Raytest, Straubenhardt, Germany). Data were tested for significant differences using two-tailed Student's t test.

Electrospray Ionization-MS Quantification of Glucosylceramides and Ceramides—Free extractable sphingolipids were analyzed with a triple quadrupole instrument (VG Micromass Model Quattro II, Cheshire, UK) equipped with a nano-electrospray source. Quantification was performed with internal standards for ceramides (Cer(d18:1,14:0), Cer(d18:1,19:0), Cer(d18:1,25:0), Cer(d18:1,31:0), and Cer(t18:0,31:0)) and glucosylceramides (GlcCer(d18:1,14:0), GlcCer(d18:1,19:0), GlcCer(d18:1,25:0), and Cer(d18:1,31:0)) according to Jennemann *et al.* (21).

After adding internal standards, samples were injected directly into the nano-electrospray ionization source of the mass spectrometer. Ceramides and glucosylceramides containing the major sphingoid base sphingosine (d18:1) were detected by precursor ion scanning with the fragment m/z +264 specific for long chain sphingoid base (d18:1) using a collision energy of 50 eV and a linear cone voltage ramp of 35 V at m/z 500 up to 65 V at m/z 1500.

Sphingolipids with a fatty acid hydroxylation shifted in the mass spectra up by 16 Da and thus could be distinguished from sphingolipids with nonhydroxylated acyl moieties. Epidermal sphingolipids with acyl chains not longer than 26 carbon atoms have been reported to basically contain α-hydroxylations, whereas ultra long chain acyl moieties (>28 carbon atoms) released from *O*-acyl esters are published to be ω-hydroxylated in skin (22–24). Thus, we grouped α-hydroxy (C16–26) and ω-hydroxy (C30–36) compounds according to the length of the acyl moieties.

Depilation—Dorsal skin of 45–46-day-old $Fa2h^{-/-}$, $Fa2h^{+/-}$ and wild-type male mice was depilated when hair follicles were in late catagen to early telogen phase of the hair cycle. Photographs were taken every day from the depilated mice, and the skin color was recorded. At 6, 10, and 20 days after depilation, mice were killed by cervical dislocation, and the depilated area of the back skin was prepared as described previously (19). One-half of the sample was homogenized in TRIzol for subsequent RNA isolation, and the other part was fixed in 4% PFA and embedded in paraffin, and sections (6 μm) were stained with H&E as described above.

Melting Point Analysis—Surface lipids were extracted by dipping mice into acetone. The acetone extract was filtered through glass wool and dried under nitrogen. After evapora-

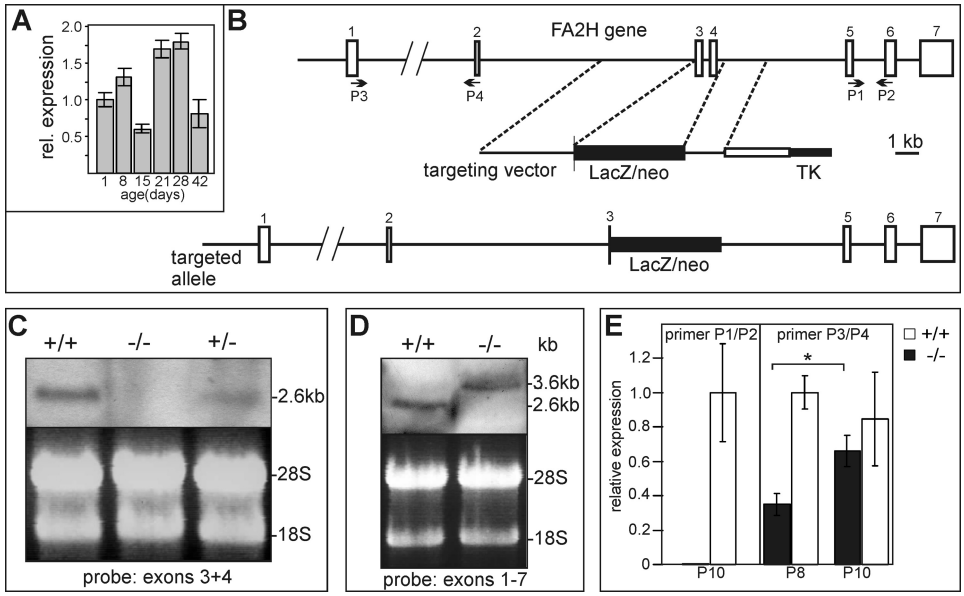

FIGURE 1. **Generation of *Fa2h*$^{-/-}$ mice.** *A,* real time RT-PCR of *Fa2h* expression in the back skin of C57BL/6 wild-type mice between postnatal days 1 and 42 showed hair cycle-dependent variation of *Fa2h* expression. *B,* schematic representation of the *Fa2h* targeting construct and the targeted allele in *Fa2h*$^{-/-}$ mice. Positions of oligonucleotides (*P1–P4*) used for RT-PCR are indicated. *C,* Northern blot analysis using an exon3/4-specific probe confirmed the absence of the *Fa2h* mRNA in murine skin. *D,* Northern blot analysis of mouse back skin using a full-length *Fa2h* cDNA probe detected the expression of the *Fa2h-Cytb5-lacZ* gene. *E,* real time PCR confirmed the absence of *Fa2h* transcripts containing exons 5 and 6 in *Fa2h*$^{-/-}$ mice and the presence of the *FA2H-Cytb5-lacZ* fusion product (containing exons 1 and 2). The transcript was significantly up-regulated during morphogenesis between P8 and P10 (*, $p < 0.05$, *t* test).

tion, the lipids were taken up in a small volume of *n*-hexane and transferred into melting point capillaries. The solvent was allowed to evaporate at 37 °C overnight. The melting point was determined using a capillary-type melting point apparatus (Buchi model 535; Büchi Labortechnik AG, Flawil, Switzerland). The temperature when the melting process started and the temperature when the surface lipid mixture appeared liquid completely were determined.

Water Repulsion Test—Mice were placed in a 425 × 265 × 150-mm plastic container containing water (temperature 35–37 °C) for 3 min and then placed on paper towels for 15 s to absorb excess water. The mice were then exposed to ambient temperature (20 °C), and their body weights were recorded for 55 min.

Semithin Sections and Electron Microscopy—Mice were killed with an overdose of anesthetics and perfused via the left ventricle with Sörensen phosphate buffer with 1% procaine followed by 6% glutaraldehyde in the same buffer. After postfixation in OsO_4, samples were dehydrated in a graded series of ethanols and embedded in 1,2,3-propanetriol glycidyl ether or Spurr's medium. Semithin sections were cut at 1 μm and stained with toluidine blue/pyronin G for light microscopy, using a Nikon 90i photomicroscope for documentation. Blocks were then trimmed down to a surface of about a square millimeter and resectioned at 70 nm; sections then contrasted with lead citrate and uranyl acetate and photographed in either a Zeiss EM 910 TEM or a JEOL 7500F SE in STEM mode.

RESULTS

Delayed Fur Emergence and Cyclic Alopecia in FA2H-deficient Mice—Fa2h is strongly expressed in murine skin (13), and its expression exhibits hair cycle-dependent changes in wild-type mice (Fig. 1*A*). *Fa2h* expression was significantly up-regulated during morphogenesis and anagen and down-regulated in telogen. To further explore the role of FA2H in skin, *Fa2h*$^{-/-}$ mice were generated by inserting a *lacZ* reporter gene into the *Fa2h* gene (Fig. 1*B*) (16). Northern blot analysis of back skin RNA from wild-type, *Fa2h*$^{+/-}$, and *Fa2h*$^{-/-}$ mice confirmed absence of the *Fa2h* mRNA in the latter, reduced expression in heterozygous mice (Fig. 1*C*), and expression of an mRNA of the expected size transcribed from the *Fa2h-Cytb5-lacZ* fusion gene (Fig. 1*D*). Absence of full-length *Fa2h* mRNA was confirmed by RT-PCR of total skin RNA (Fig. 1*E*). Exon 1- and 2-specific primers confirmed expression of the *Fa2h-Cytb5-lacZ* fusion gene in *Fa2h*$^{-/-}$ mice, which was significantly up-regulated between P8 and P10, in contrast to the *Fa2h* mRNA of wild-type mice (Fig. 1*E*).

Newborn *Fa2h*$^{-/-}$ mice were indistinguishable from their wild-type littermates up to an age of 4–5 days. The skin of *Fa2h*$^{-/-}$ mice at 5–7 days of age, however, often appeared more flaky compared with wild-type or heterozygous mice (data not shown). The first fur became visible at postnatal day 6 in wild-type and heterozygous mice. In contrast, *Fa2h*$^{-/-}$ littermates showed a delay in fur development by 2 days, and the first fur became visible at day P8 to P9 (Fig. 2*A*). Thereafter, hair growth proceeded normally, although the fur appeared more irregular in *Fa2h*$^{-/-}$ mice with an apparently lower hair density (Fig. 2*B*). The fur of young *Fa2h*$^{-/-}$ mice was in addition less soft and glossy, and the hair seemed to be covered with a film of white material, and chunks of different sizes were detectable on the skin and hair. Some *Fa2h*$^{-/-}$ mice exhibited significant hair loss of their back skin in the first telogen (data not shown). During subsequent hair cycles, however, all *Fa2h*$^{-/-}$ mice showed repeated loss of their back and ventral skin hair (Fig. 2*C*, and data not shown). According to the pink skin color of the

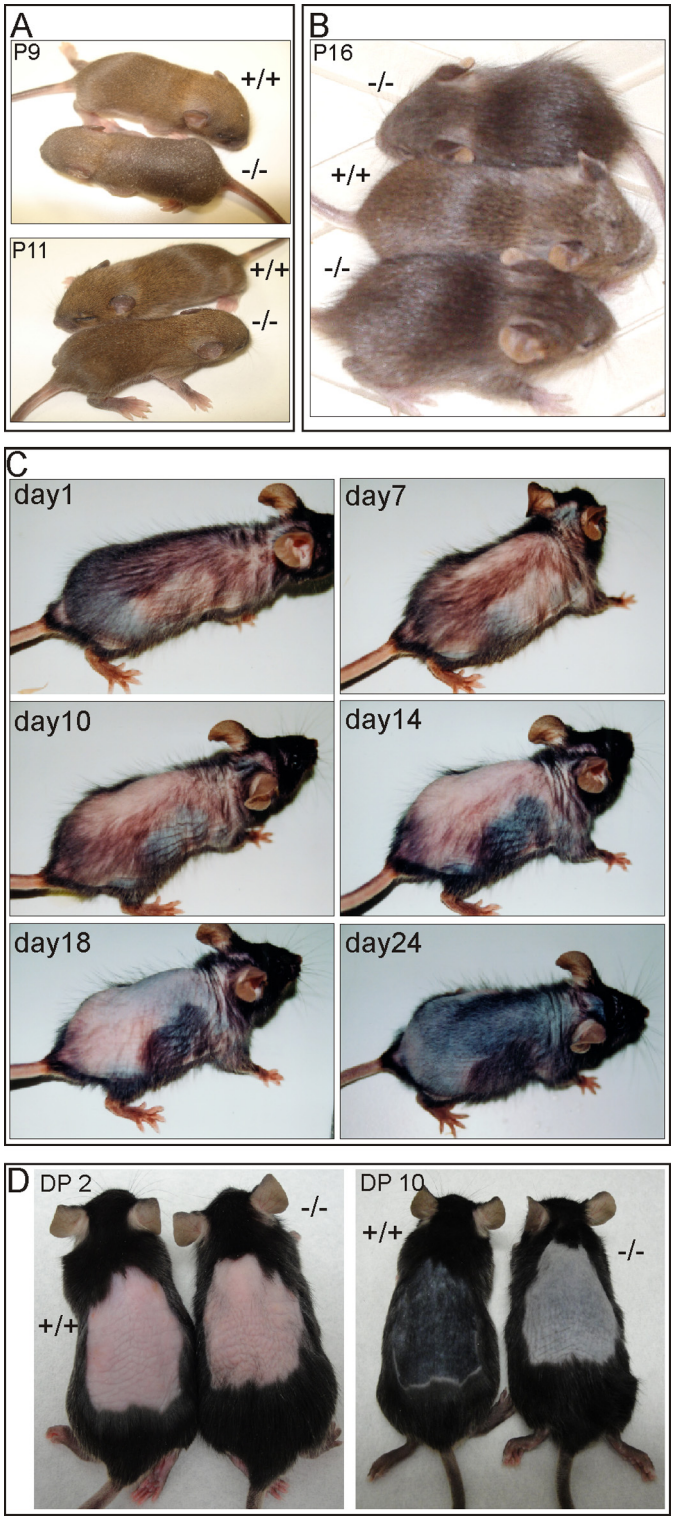

FIGURE 2. **Delayed fur development and cyclic alopecia in *Fa2h*$^{-/-}$ mice.** *A*, *Fa2h*$^{+/+}$ and *Fa2h*$^{-/-}$ littermates at postnatal days 9 and 11. Development of the fur is delayed by about 2 days. *B*, at the end of hair follicle morphogenesis (P16), fur of *Fa2h*$^{-/-}$ mice appears almost normal, although the hair density appear to be lower compared with their wild-type littermates. *C*, photographs were taken from a 6-month-old male *Fa2h*$^{-/-}$ mouse over a period of 24 days to demonstrate the cyclic alopecia. *D*, visual inspection of male mice depilated at an age of 45, 2 (DP2), and 10 days (DP10) after depilation showed that development of the new fur was significantly delayed.

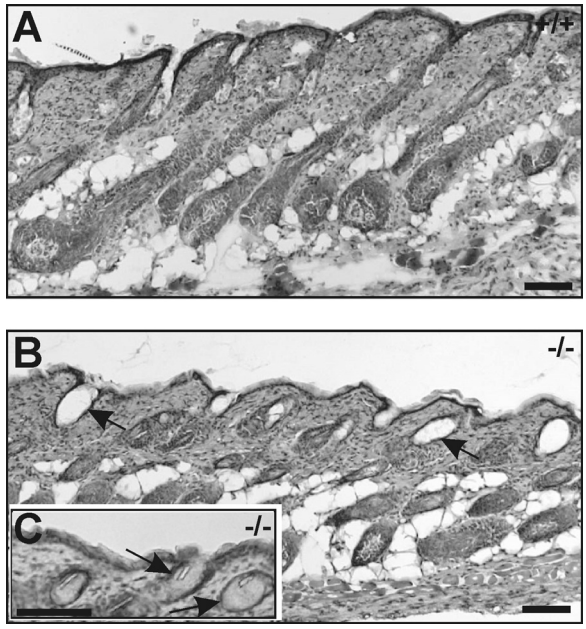

FIGURE 3. **Dilated follicle ostia in *Fa2h*$^{-/-}$ mice.** Skin paraffin sections of 4-week-old wild-type (*A*) and *Fa2h*$^{-/-}$ (*B*) mice indicated that follicle ostia were dilated in the latter (*arrows*). *C*, analysis of cryosections showed that the hair canals of *Fa2h*$^{-/-}$ mice were filled with sebum (*arrows*). *Scale bars*, 100 μm.

areas showing hair loss, this apparently occurred in telogen. As hair loss appeared to proceed relatively slowly (within several days), the fact that only a fraction of 4-week-old *Fa2h*$^{-/-}$ mice exhibited severe alopecia in the first telogen may be explained by the short first telogen phase (1–2 days (25)).

The regeneration capacity of hair follicles was examined after inducing anagen by depilation of the back skin in 45–46-day-old male mice (with hair follicles in the late catagen to early telogen phase, as indicated by the pink color of the back skin before depilation). Emergence of the new fur was delayed by about 2–3 days in *Fa2h*$^{-/-}$ mice (range, 12–14 days after depilation in *Fa2h*$^{-/-}$ compared with 9–12 days in wild-type and heterozygous controls), resembling the delay in fur development during morphogenesis (Fig. 2*D*). According to histological analyses and the changes in skin color, anagen induction was unaffected in *Fa2h*$^{-/-}$ mice, suggesting that not a delay in the induction of hair growth but a retention of the hair fiber exit was responsible for delayed emergence of the fur.

Histological Analyses—In contrast to wild-type mice, the follicle ostia of *Fa2h*$^{-/-}$ mice appeared dilated in the telogen and early anagen phase (Fig. 3, *A* and *B*). Analysis of cryosections (Fig. 3*C*) revealed that the dilated hair canals were filled with sebum, which was also stainable with oil red (data not shown). Analysis at higher resolution of semithin section by light and electron microscopy revealed that large "sebum plugs" appear to be liberated "*en bloc*" from the SG, whereby the cell membranes were often still discernible in cells that had already lost their nucleus, indicating that these sebum plugs were released before apoptosis during holocrine secretion was complete (Fig. 4, *A*–*E*). This might be explained by altered sebum composition in *Fa2h*$^{-/-}$ mice, causing a significant increase in the melting temperature (as shown below), or by an as yet unexplained impact of altered sebum composition on the process of holo-

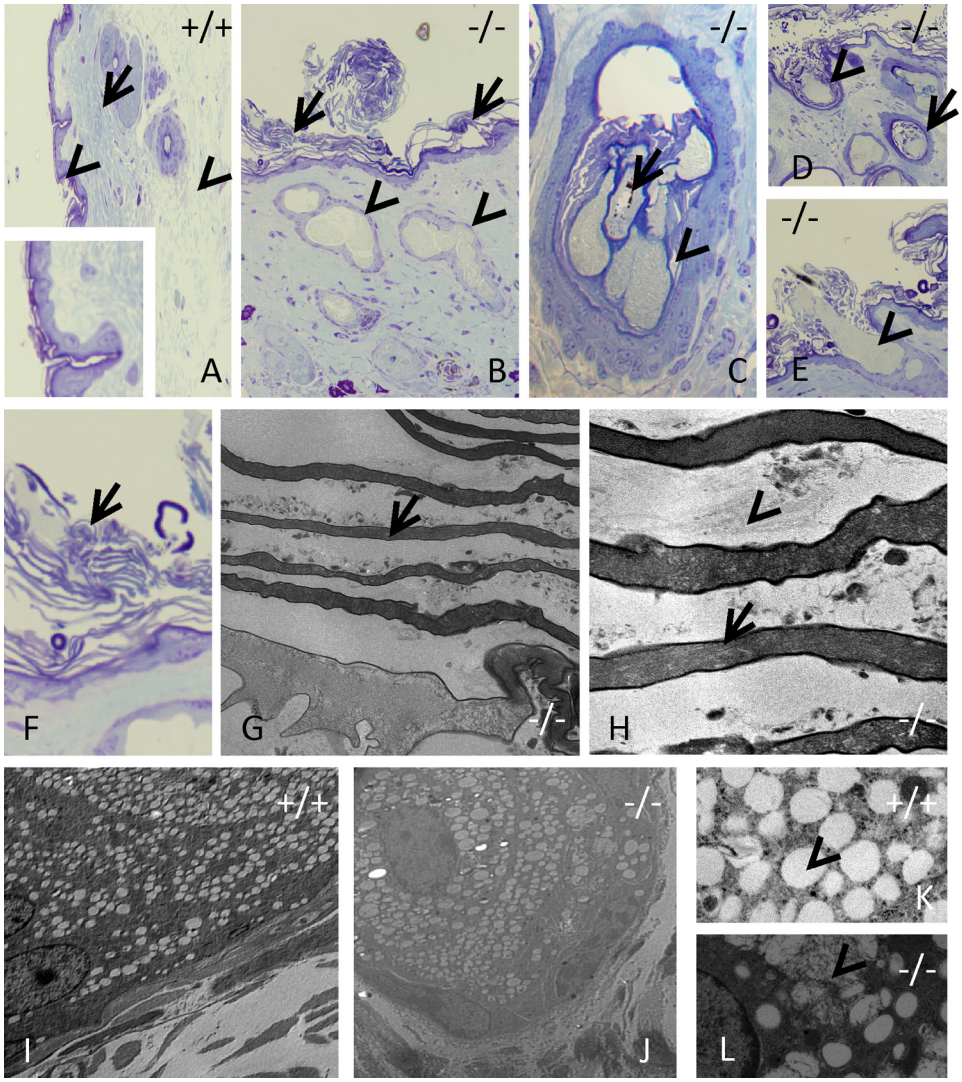

FIGURE 4. **Histological and ultrastructural analysis.** *A* and *B,* low magnification of the skin of *Fa2h*$^{-/-}$ mice. *B* is characterized by distended follicles from the level of SG upwards (*arrowheads* in *B,* compare with wild type in *A*). At the same time, the skin surface is characterized by multiple layers of loosely attached keratinized cells at the outer aspect of the stratum corneum (*arrows* in *B*). *C* and *I–L,* overall morphology of both the sebaceous glands (*C*) as well as the ultrastructure of sebocytes (*I–L*) did not show overt specific alterations (note that the ultrastructure of most lipid droplets is unchanged; however, some droplets appear to be irregularly shaped with an unusual internal structure (*arrowhead* in *L*)). Distal to the juncture of the sebaceous glands with the hair follicle, the hair shafts are either absent or appear to be compressed with obvious signs of degeneration (*arrow* in *C*). *D* and *E,* follicle ostia are filled with plugs of sebum (*arrowhead*) and hair shaft and root sheath debris (*arrow*). It is striking that the sebum apparently does not readily spread onto the surrounding skin but projects out of the follicle ostia as elongated pear-shaped masses, sometimes with an internal segmentation reminiscent of sebocyte cell borders. *F–H,* outside of the compact stratum corneum, the skin in *Fa2h*$^{-/-}$ mice is covered by a thick coat of multiple layers of fully keratinized cells (*arrows*) separated by almost regular spaces filled with granular material of unknown origin (*arrowhead* in *H*).

crine secretion itself. As the dilated follicula ostia appeared to be filled with sebum that was less mobile either due to its composition (see below) and/or partial presence of cell remnants, the anchoring of the club hair may be affected, and the hair may be dislodged by scratching (or the hair may be lost when the sebum plugs are dislodged). The delay in emergence of the fur during morphogenesis and anagen may also be caused by the sebum plugs blocking the hair tip. The morphology of the sebaceous glands did not show overt specific alterations (Fig. 4*C*). Outside of the compact stratum corneum, the skin in *Fa2h*$^{-/-}$ mice was covered by a thick coat of multiple layers of fully keratinized cells separated by almost regular spaces filled with granular material of unknown origin (Fig. 4, *F–H*).

The ultrastructure of most lipid droplets was unchanged in *Fa2h*$^{-/-}$ mice (Fig. 4, *I* and *J*), although some droplets appeared to be irregularly shaped with an unusual internal structure (Fig. 4*L*, *arrowhead*), which may be the result of altered lipid composition (see below). Distal to the juncture of the sebaceous glands with the hair follicle, the hair shafts are either absent or appear to be compressed with obvious signs of degeneration (Fig. 4*C*, *arrow*).

Analysis of Skin and Epidermal Sphingolipids—To examine whether the observed phenotype is accompanied by the expected changes in sphingolipid composition (lack of 2-hydroxylated sphingolipids), total lipid extracts were prepared from epidermis of young (P10) and adult (1-year-old) *Fa2h*$^{-/-}$ mice and *Fa2h*$^{+/-}$ mice. Unexpectedly, thin layer chromatography (TLC) of epidermal lipids revealed no obvious difference between *Fa2h*$^{-/-}$, *Fa2h*$^{+/-}$ mice (Fig. 5*A*), and wild type (data not shown). In particular, we found no reduction in the amount

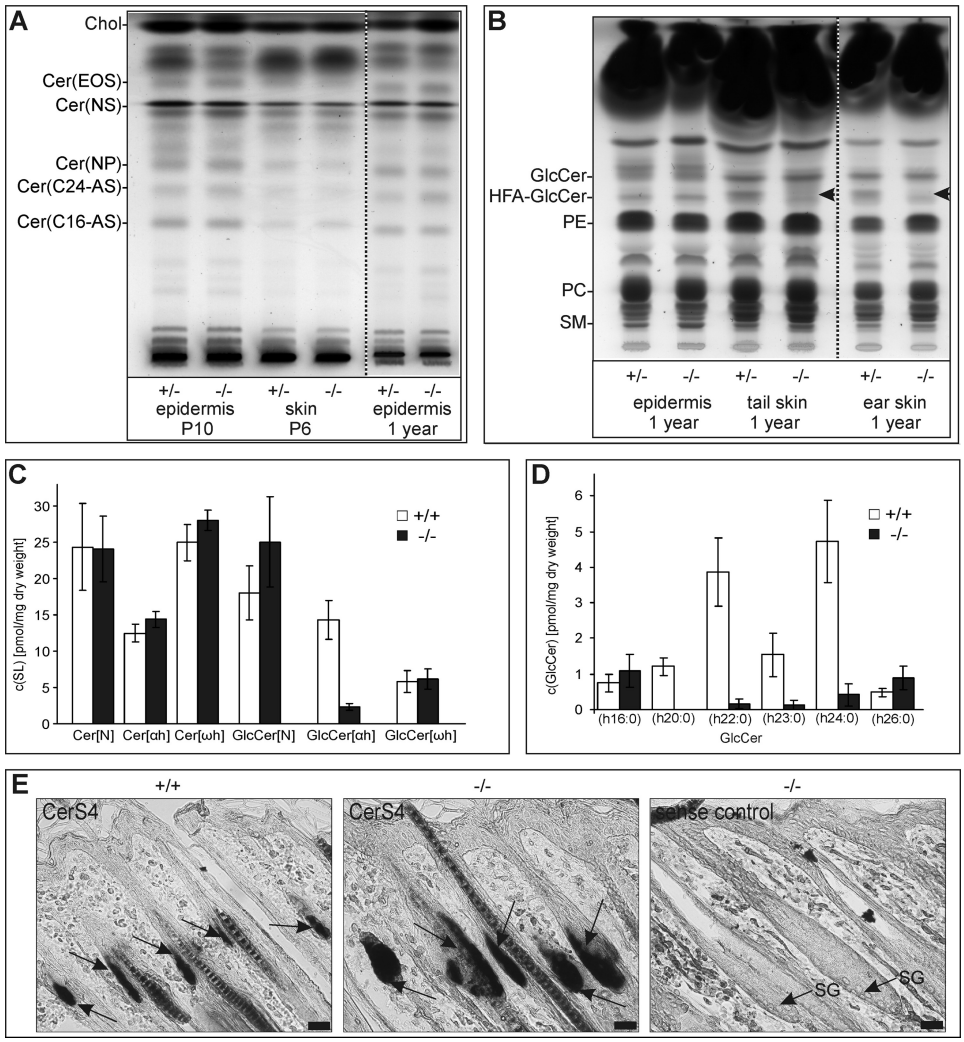

FIGURE 5. **Analysis of epidermal and skin sphingolipids.** *A,* TLC analysis of epidermal ceramides isolated from the skin of 6- and 10-day-old and 1-year-old mice showed no significant differences between *Fa2h*$^{+/-}$ and *Fa2h*$^{-/-}$ mice. In particular, 2-hydroxylated ceramides (*Cer*(*C16-AS*)) were present in *Fa2h*$^{-/-}$ mice, which was confirmed by mass spectrometry (data not shown). *Chol*, cholesterol. *B,* in contrast to epidermal lipids, reduced levels of 2-hydroxylated GlcCer were evident in total skin from tail and ears of *Fa2h*$^{-/-}$ mice (*arrowheads*). Abbreviations used are as follows: *GlcCer,* nonhydroxylated GlcCer; *HFA-GlcCer*, 2-hydroxylated GlcCer; *PE*, phosphatidylethanolamine; *PC,* phosphatidylcholine; *SM*, sphingomyelin. *C,* mass spectrometry of sphingolipids (*SL*) isolated from the auricles showed a significant decrease (*t* test, $p < 0.05$) in the amount of 2-hydroxylated GlcCer, but not 2-hydroxylated ceramides, in *Fa2h*$^{-/-}$ mice when compared with wild-type controls (+/+). According to the precursor ion mode selected (*m/z* +264), only ceramides and GlcCer with a d18:1-sphingoid base were measured. Abbreviations used are as follows: *Cer,* ceramide; *GlcCer,* glucosylceramide; *N,* nonhydroxylated; *SL*, sphingolipid; *So,* sphingosine; *αh,* 2-hydroxylated; *ωh*, *ω*-hydroxylated. *D,* further analysis of 2-hydroxylated (h) GlcCer species revealed absence of h20:0-GlcCer and significantly reduced levels of h22:0, h23:0, and h24:0-GlcCer (*t* test, $p < 0.05$). In contrast the concentrations of h16:0- and h26:0-GlcCer were not significantly changed in *Fa2h*$^{-/-}$ mice. *E, in situ* hybridization of back skin cryosections with ceramide synthase 4 (*CerS4*) cRNA antisense probes showed specific expression in the SG (indicated by *arrows*), whereas *CerS4* expression was undetectable in keratinocytes. *CerS4* expression was strongly increased in *Fa2h*$^{-/-}$ mice, apparently because of SG enlargement. A CerS4 cRNA sense control showed no specific hybridization signals (SG are marked by *arrows*). *Scale bars,* 20 μm.

of 2-hydroxylated ceramides (Fig. 5*A*) and 2-hydroxylated glucosylceramides (HFA-GlcCer) (Fig. 5*B*). The presence of 2-hydroxylated sphingolipids in *Fa2h*$^{-/-}$ epidermis was further confirmed by mass spectrometry (data not shown). Furthermore, no significant changes in the level of covalently bound (*ω*-hydroxylated) ceramides and glucosylceramides were observed by TLC analysis (data not shown).

In another set of experiments, lipid composition was examined in total skin samples. To reduce the amount of triglycerides derived from the subcutis, auricles, and tail skin, samples were used for these analyses. Again, no obvious changes in the amount of hydroxylated ceramides were observed by TLC and mass spectrometry (Fig. 5*C*, and data not shown). However, TLC analysis showed a significant reduction in the amount of HFA-GlcCer in *Fa2h*$^{-/-}$ total skin (Fig. 5*B*), which was confirmed by mass spectrometry (Fig. 5*C*). Mass spectrometry of individual GlcCer species further revealed normal levels of hydroxylated C16- and hydroxylated C26-GlcCer, whereas hydroxylated C22- and hydroxylated C24-GlcCer were significantly reduced, and hydroxylated C20-GlcCer was undetectable in *Fa2h*$^{-/-}$ mice (Fig. 5*D*). Taken together, the above results clearly demonstrate that only a subset of 2-hydroxylated fatty acids present in sphingolipids of murine skin was synthesized by FA2H.

Fa2h Expression in Murine Skin Is Restricted to SG—To identify the cell types expressing *Fa2h* in murine skin, X-Gal staining of embryos, back skin, and ears from mice of all three genotypes was performed at different ages. Whole mount staining

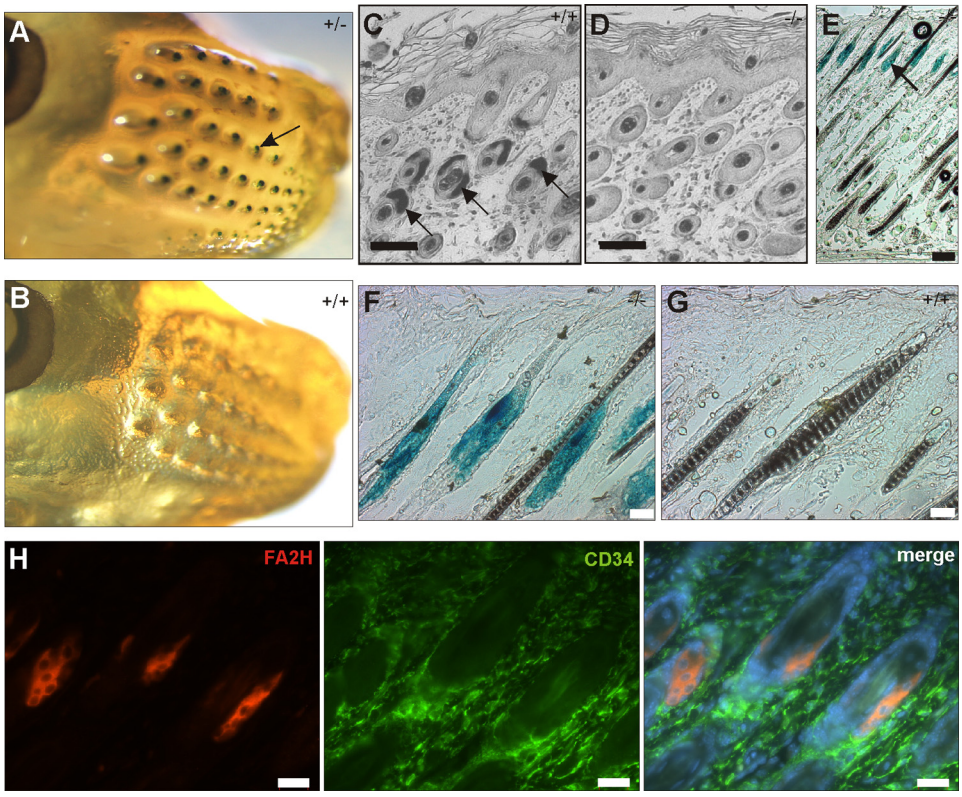

FIGURE 6. **Fa2h is specifically expressed in SG.** *A* and *B,* whole mount X-Gal staining of E16.5 embryos revealed the first FA2H-positive cells at the vibrissae anlagen. According to their relative position, these cells most likely were sebocytes. *C* and *D, in situ* hybridization of P6 back skin showed Fa2h expression in sebaceous glands of wild-type (*arrows* in *C*) but not $Fa2h^{-/-}$ mice (*D*). SG-specific expression of *Fa2h* was confirmed by X-Gal staining of P10 (*E*) and adult skin (*F* and *G*). *H,* costaining of FA2H and CD34 (in wild-type mice) indicated that the CD34-positive stem cells of the bulge region do not express detectable amounts of FA2H. *Scale bars,* 20 μm in *C, D,* and *F–H,* and 100 μm in *E*.

of $Fa2h^{+/-}$ embryos at E16.5 revealed the first lacZ-positive cells at the vibrissae anlagen, possibly sebocytes (Fig. 6, *A* and *B*). At P10 and in adult mice, LacZ-positive cells were restricted to the SG (Fig. 6, *E–G*). These results were confirmed by *in situ* hybridization. Fa2h antisense probes gave strong expression signals exclusively in the SG in wild-type mice but not in $Fa2h^{-/-}$ mice (Fig. 6, *C* and *D*). Immunostainings with an FA2H-specific antiserum detected the FA2H protein only in the SG (Fig. 6*H*). There was no costaining of FA2H with antibodies against CD34, indicating that stem cells of the bulge region do not express *Fa2h* (Fig. 6*H*). The specific expression of *Fa2h* in sebocytes, but not in keratinocytes, the cells mainly responsible for the synthesis of 2-hydroxylated ceramides in the skin, is in line with the observed changes in the sphingolipid profiles described above. The specific down-regulation of hydroxylated C20-GlcCer to undetectable levels (see above) is in accordance with the observation that the ceramide synthase 4, which among all ceramide synthases has the highest preference for C20:0-coenzyme A (26, 27), is strongly expressed in SG but is not detectable in keratinocytes (Fig. 5*E*).

Altered Composition and Melting Point of Surface Lipids in FA2H-deficient Mice—Analysis of total skin lipids revealed further changes in the most apolar lipids, suggesting altered sebum composition (data not shown). Surface lipids, which are mainly derived from sebum (7), were extracted from $Fa2h^{-/-}$ and control mice using acetone. Mouse sebum contains large amounts of type II wax diester (formed by the condensation of two acyl residues with a 1,2-diol), wax monoesters, and sterol esters (Fig. 7*A*). TLC analysis (Fig. 7, *A* and *B*) revealed that the total amount of wax diesters was strongly reduced by about 70–75% in 10-day-old $Fa2h^{-/-}$ mice, whereas wax monoesters were significantly (3–4-fold at P10) increased. Comparable changes in sebum composition were found in adult $Fa2h^{-/-}$ mice (data not shown). In addition, the concentration of cholesterol and free fatty acids were slightly but significantly increased (Fig. 7*B*).

To examine whether sebum plugs in the hair canal observed in histological preparations (see Fig. 4) might be due to altered physicochemical properties of the sebum, we determined the melting points of surface lipids isolated from wild-type and $Fa2h^{-/-}$ mice. Melting begins at 37 °C in the case of wild-type sebum, whereas it was increased to more than 50 °C in the case of $Fa2h^{-/-}$ mice (Fig. 7*C*), suggesting a much more waxy appearance, which is in line with the appearance of the hair and the histological data (see above). Because the oily or waxy surface produced by the sebum lipids is important for water repulsion (9), we examined the possibility of altered water retention in $Fa2h^{-/-}$ mice. A water repulsion test, however, indicated normal ability of $Fa2h^{-/-}$ mice to repel water (data not shown).

Enlarged SG during Morphogenesis and Anagen in FA2H-deficient Mice—Histological examinations indicated that the size of SG in $Fa2h^{-/-}$ mice increased considerably during morphogenesis (Fig. 8*A*) and depilation-induced anagen (Fig. 8*B*). The area occupied by SG in paraffin sections was significantly increased 10 days after depilation (Fig. 8*B*). Staining of the proliferation marker Ki67 indicated elevated numbers of proliferating undifferentiated sebocytes in the outer area of the SG (Fig.

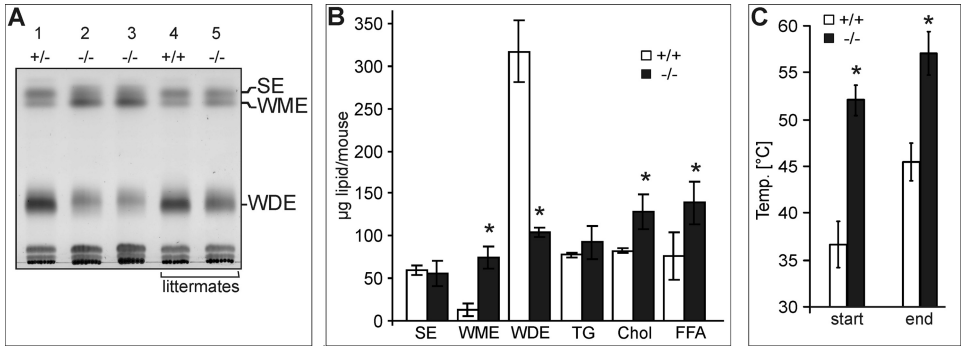

FIGURE 7. **Analysis of skin surface lipids.** *A,* surface lipids were extracted from 10-day-old $Fa2h^{+/-}$ (*lane 1*), $Fa2h^{+/+}$ (*lane 4*), and $Fa2h^{-/-}$ (*lanes 2, 3,* and *5*) mice using acetone. Note that lipids shown in *lanes 4* and *5* were obtained from littermates. TLC analysis showed increasing amounts of wax monoesters (*WME*), but reduced amounts of wax diesters (*WDE*) in surface lipids of $Fa2h^{-/-}$ mice. The concentration of sterol esters (*SE*) was not changed. *B,* densitometric analysis of extracted surface lipids showed a significant reduction in wax diester type II and an increase in wax monoesters in $Fa2h^{-/-}$ mice. In addition, the amount of cholesterol (*Chol*) and free fatty acids (*FFA*) were significantly increased in $Fa2h^{-/-}$ mice (*, $p < 0.05$, *t* test). Data shown are the means ± S.D. ($n = 4$). Abbreviations used are as follows: *SE,* sterol esters; *WME,* wax monoesters; *WDE,* wax diesters; *TG,* triglycerides; *Chol,* cholesterol; *FFA,* free fatty acids. *C,* melting point analysis of total surface lipids from adult $Fa2h^{-/-}$ and wild-type mice. The temperatures when the lipid extracts starts to melt (*start*) and are completely fluid (*end*) were determined. Data shown are the mean ± S.D. from three independent experiments (*, $p < 0.05$, *t* test).

8*C*, *arrowhead*). The number of Ki67-positive cells per SG was increased in $Fa2h^{-/-}$ mice (mean ± S.D. = 21.1 ± 2.3; $n = 3$) compared with controls (mean ± S.D. = 7.9 ± 2.8; $n = 3$) at P10. In addition, the number of Ki67-positive cells was also increased in the upper outer root sheath (ORS) (*arrows* in Fig. 8*C*), *i.e.* cells that do not show detectable *Fa2h* expression. Furthermore, BrdU labeling showed an increased number of dividing cells in the basal layer of the SG (Fig. 8*D*). Thus, FA2H deficiency causes an enlargement of SG during the growing phase of the hair cycle caused by the hyperproliferation of sebocytes/sebocyte precursors.

To further explore the pathway leading to enlarged SG, microarray hybridization experiments were performed using the back skin of P10 male mice. A total of 343 probe sets were differentially expressed (≥2-fold change; $p < 0.05$) in $Fa2h^{-/-}$ mice compared with wild-type littermates (370 probe sets were differentially expressed in $Fa2h^{-/-}$ when compared with heterozygous $Fa2h^{+/-}$ mice; the overlap between the groups of differentially expressed genes in the two comparisons was 273 probe sets). Several genes up-regulated in $Fa2h^{-/-}$ (compared with wild type and $Fa2h^{+/-}$) have been previously shown or are expected to be expressed in SG, *e.g.* PPARγ, stearoyl-CoA desaturase (Scd)-1, Scd-3, and ceramide synthase ceramide synthase 4 (see above) (Table 2; see also Fig. 9*E*), and also diacylglycerol acyltransferase-1 (Dgat1) and fatty acyl-CoA dehydrogenase-1 and -2 (Far1 and Far2), *i.e.* enzymes involved in wax mono- and diester synthesis in SG (28, 29). The latter finding suggests that reduced wax diester content in $Fa2h^{-/-}$ sebum is not caused by reduced expression of these enzymes but most likely results from inefficient diol synthesis caused by reduced fatty acid 2-hydroxylase activity. The keratin K6a, which is specifically expressed in the suprabasal layer of SG (30), was significantly up-regulated in $Fa2h^{-/-}$ mice, in line with sebocyte hyperproliferation (Table 2). Up-regulation of several sebocyte markers, Scd1, Scd3, and PPARγ, was confirmed by quantitative real time RT-PCR (Fig. 9).

Several epidermal growth factor (EGF)/ErbB receptor ligand genes (Epigen (*Epgn*), β-cellulin, heparin-binding EGF-like growth factor, and neuregulin-4 (*Nrg4*)) were up-regulated between 2.4- and 9.4-fold in $Fa2h^{-/-}$ mice. Quantitative real time RT-PCR confirmed this (Fig. 9, *A* and *D*) and in addition showed that Epgn was strongly up-regulated during morphogenesis between days 6 and 10, and also during depilation induced anagen, in accordance with the SG enlargement. *Epgn* expression was not significantly increased in telogen skin of $Fa2h^{-/-}$ mice (Fig. 9*A*). Whereas the 2–3-fold up-regulation of several SG genes at P10 reflects the increase in the SG size, *Epgn* was already strongly up-regulated between P6 and P8, suggesting that *Epgn* up-regulation may cause sebocyte hyperproliferation and SG enlargement. *In situ* hybridization confirmed the specific up-regulation of *Epgn* in the basal layer of the SG and some adjacent cells of the ORS (Fig. 9*B*). Sebocytes express EGF receptors, and in line with our data, the transgenic overexpression of *Epgn* causes a specific enlargement of the SG (31). Interestingly, both methods, microarray and real time PCR, failed to detect changes in the expression of melanocortin 5 receptor (*Mc5r*) (Fig. 9*D*), a specific marker for fully differentiated lipid-laden sebocytes (32). This might indicate that the final stage of sebocyte differentiation was impaired in $Fa2h^{-/-}$ mice.

DISCUSSION

Currently, FA2H is the only known mammalian enzyme catalyzing the synthesis of straight 2-hydroxylated fatty acids (14). It was therefore unexpected that in murine skin *Fa2h* is specifically expressed in SG. Deficiency in *Fa2h* caused a delay in emergence of the fur during morphogenesis and depilation-induced anagen and a cyclic alopecia. These observations underline the importance of the SG in hair follicle homeostasis. The major function of SG is the production of sebum, which contains various lipids and is released into the hair canal by holocrine secretion (5, 6). Sebum components have antimicrobial activity (33, 34), and sebum is protective against oxidative stress and UVB (35, 36). Beside these protective roles, there is evidence for additional functions of SG in hair follicle homeostasis. This conclusion is mainly based on the analysis of the *asebia* mouse (36, 37), which has a deficiency in the *Scd1* gene (encoding the desaturase responsible for C18:1-CoA synthesis), causing a degeneration of SG (8, 36, 37). This is accompanied by prolonged hair cycle phases, including the prolonged growing phase of hair follicles and alopecia (38, 39). It has been proposed

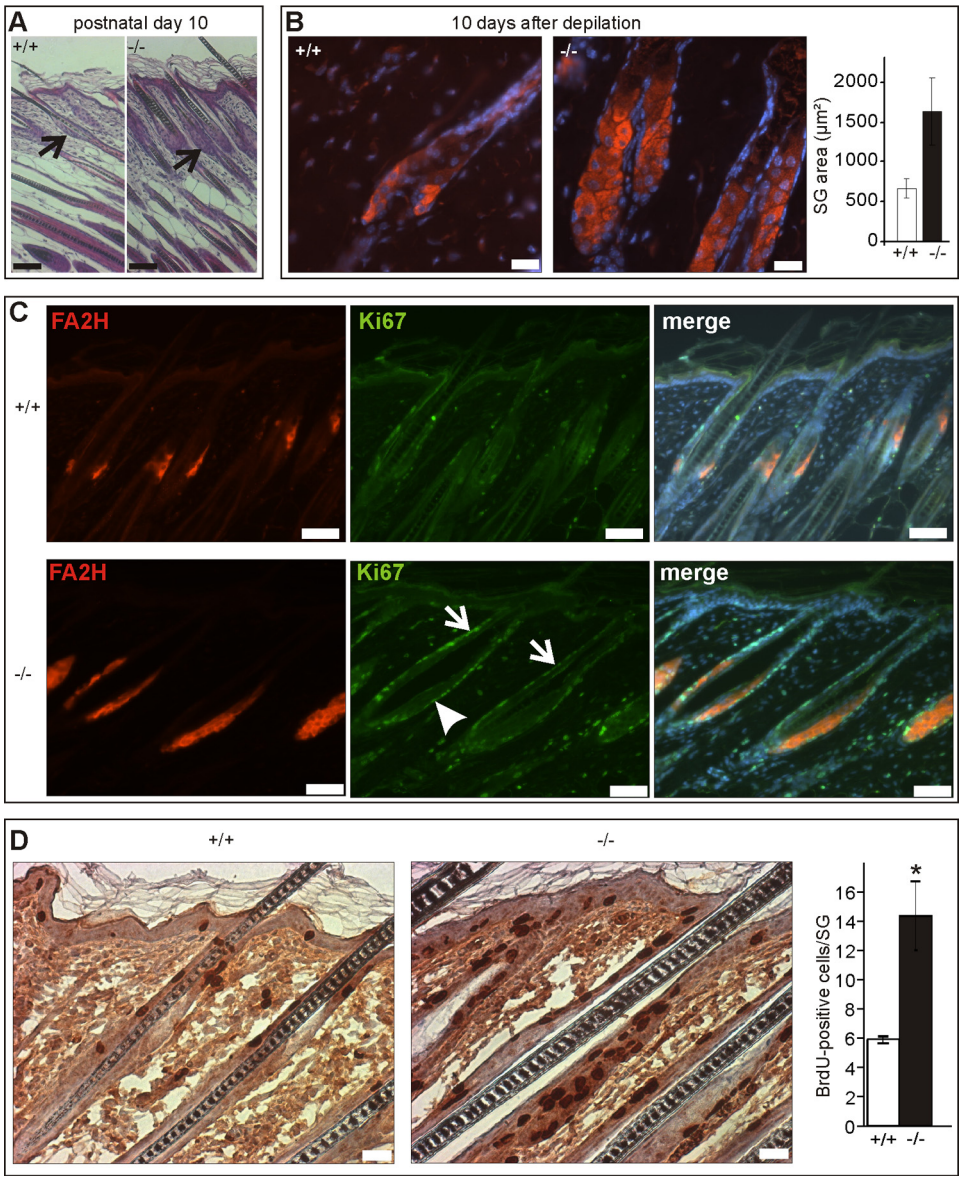

FIGURE 8. ***Fa2h*$^{-/-}$ mice have enlarged SG during morphogenesis and anagen.** *A,* H&E staining of P10 back skin showed significantly enlarged SG (*arrows*) in *Fa2h*$^{-/-}$ mice. *B,* SG were also enlarged in *Fa2h*$^{-/-}$ mice during depilation-induced anagen. The area occupied by individual SG were determined on paraffin sections stained with FA2H antiserum. *C,* costaining of P10 skin with antibodies against FA2H and Ki67 revealed increased number of proliferating cells in the basal layer of the SG (*arrowhead*) but also in adjacent cells of the upper ORS (*arrows*). *D,* hyperproliferation of basal sebocytes at postnatal day 10 was confirmed by BrdU labeling. *Asterisk* indicates a statistically significant difference ($p < 0.05$; *t* test). *Scale bars,* 50 μm (*A* and *C*) and 20 μm (*B* and *D*).

that many (scarring) alopecias of unknown origin might be caused by primary defects in the SG (10). This view is also supported by the observation that SG degeneration is an early event in chemotherapy-induced alopecia, which appears to precede hair loss (40).

FA2H Is Involved in Synthesis of HFA Sphingolipids and Wax Diesters in SG—Although deficiency in FA2H results in complete absence of HFA sphingolipids in the nervous system (16), we show here that synthesis of HFA sphingolipids in the mouse epidermis is independent of *Fa2h* expression. In contrast, *Fa2h* gene silencing in human keratinocyte cultures inhibited *Fa2h* expression and lamellar body formation in a previous study, suggesting an important role of FA2H-derived 2-hydroxylated sphingolipids in the formation of the skin permeability barrier (15). Possibly, *Fa2h* expression differs between mouse and human skin. For example, lack of wax diesters in human sebum may indicate absence of *Fa2h* expression in human SG, and in human keratinocytes FA2H may be responsible for HFA sphingolipid synthesis. However, normal fatty acid 2-hydroxylase activity in skin fibroblasts of human patients with FA2H deficiency (41), which causes a leukodystrophy with spastic paraparesis (41, 42), argues against this possibility and clearly demonstrates that also human skin contains at least one other fatty acid or fatty acyl-CoA 2-hydroxylase enzyme. The nature of the enzyme responsible for synthesis of HFA sphingolipids in keratinocytes is not known. The peroxisomal phytanoyl-CoA hydroxylase is involved in the degradation of branched fatty acids by α-oxidation (43), but it is not clear whether phytanoyl-CoA hydroxylase also hydroxylates straight chain acyl-CoA (44, 45). Likely candidate enzyme(s) involved in the synthesis of

TABLE 2

Microarray analysis

Values indicate relative expression levels in male *Fa2h*$^{-/-}$ back skin at postnatal day 10, compared with wild-type.

Keratins		
1451551_at	K16	0.5
1427700_x_at	K6a	2.8–3.1[a]
1423952_a_at	K7	5.7
ErbB receptor signaling		
1421161_at	Betacellulin (Btc)	2.4
1418350_at	HB-EGF	2.4–3.1[a]
1449994_at	Epigen (Epgn)	9.4
1421681_at	Neuregulin 4 (Nrg4)	5.1
SG marker		
1426960_a_at	Fa2h	0.0 (absent)
1420715_a_at	Pparγ	2.5
1415965_at	Scd1	2.6
1423366_at	Scd3	0.13–0.26[a,b]
1417781_at	CerS4/Lass4	3.5–4.4
Synthesis of sebum lipids		
1417695_a_at	Sterol *O*-acyltransferase 1	2.5–3.0[a]
1418295_s_at	Dgat1	2.4
1435621_at	Far2	3.3–5.2[a]
1426369_at	Far1	2.4–4.7*

[a] Range for up-/down-regulated genes is represented by more than one probe set on the microarray.

[b] Note that the apparent down-regulation of Scd3 could not be confirmed by real time RT-PCR (see Fig. 9*E*).

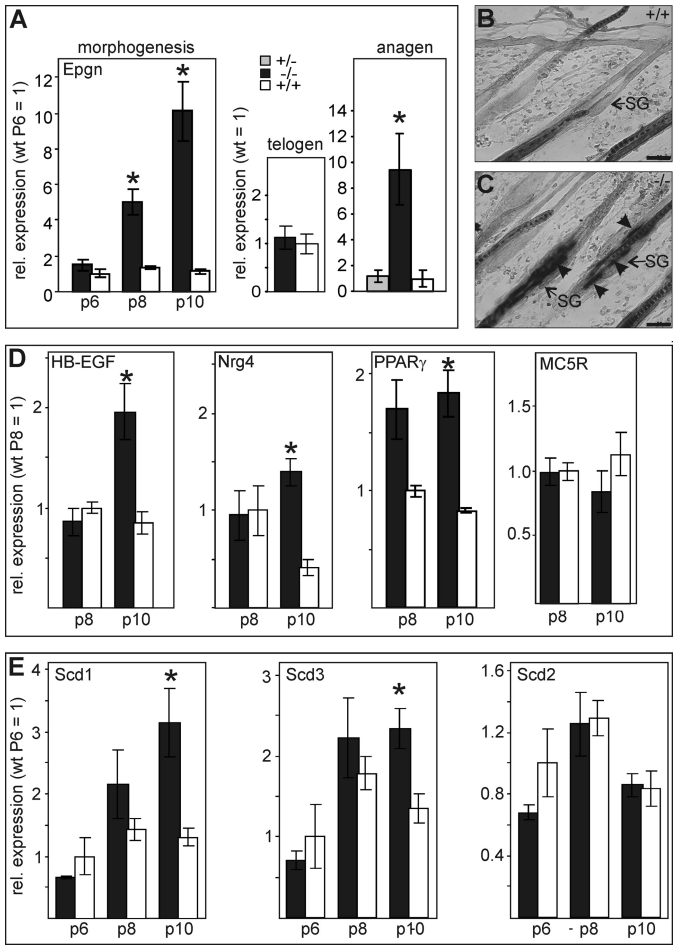

FIGURE 9. **Transient up-regulation of epigen during morphogenesis and anagen.** *A,* epigen (*Epgn*) was significantly up-regulated between postnatal days 6 and 8 in the back skin of *Fa2h*$^{-/-}$ mice (*black bars*). In telogen skin, *Epgn* expression was again down-regulated, and no significant difference between wild-type and *Fa2h*$^{-/-}$ mice was observed. A similar up-regulation of *Epgn* in *Fa2h*$^{-/-}$ mice was detected in 7-week-old *Fa2h*$^{-/-}$ mice following depilation-induced anagen. *B* and *C, in situ* hybridization confirmed up-regulation of *Epgn* expression (*arrowheads*). SG are marked by *arrows*. *Scale bars,* 40 μm (*B* and *C*). *D,* real time RT-PCR showed an approximate 2-fold up-regulation of other ErbB2 ligands, like heparin-binding EGF-like growth factor and Nrg4, confirming microarray hybridization experiments (see Table 2). *E,* in accordance with the hyperproliferation of sebocytes and enlarged SG, and SG markers (*Scd1*, *Scd3*, and *PPARγ*) were up-regulated. As a control, expression of *Scd2*, which is not expressed by sebocytes, was not changed significantly. Notably, *Mc5r*, a marker for terminally differentiated lipid-laden sebocytes, was not significantly up-regulated, which may indicate an insufficient terminal differentiation of sebocytes. Abbreviations used are as follows: *Scd1,-2,-3*, stearoyl-CoA desaturase-1, -2, and -3; *Epgn,* epigen; *Nrg4*, neuregulin-4; *HB-EGF*, heparin binding EGF; *PPARγ*, peroxisome proliferator-activated receptor-γ; *Mc5r*, melanocortin 5 receptor. Data were analyzed by the $2^{-\Delta Ct}$ method using ubiquitin C (*Ubc*) as a housekeeping control. The mean expression of wild type at P6 or P8 was set to 1. Shown are the means ± S.E. (n = 3–4). *Asterisks* indicate a statistically significant difference (*, $p < 0.05$; *t* test).

HFA sphingolipids in keratinocytes include members of the cytochrome P450 family, some of which are strongly expressed in skin (46), although there is currently no experimental evidence to support this hypothesis.

All of the six known mammalian ceramide synthases can use 2-hydroxylated acyl-CoA as substrate (47), although substrate specificity of ceramide synthases differs considerably with respect to the acyl chain length. C20-acyl-CoA is a substrate for CerS2, -3, and -4, among which CerS4 has the highest preference for C20-acyl-CoA (26, 27). Absence of hydroxylated C20:0-GlcCer in *Fa2h*$^{-/-}$ total skin samples, together with the SG-specific expression of CerS4, suggests therefore that 2-hydroxylated sphingolipids are absent in SG in *Fa2h*$^{-/-}$ mice. Normal levels of hydroxylated C16:0 and hydroxylated C26:0 GlcCer may be due to the relatively high levels of these lipids outside SG. However, the massive reduction in the total amount of HFA-GlcCer in *Fa2h*$^{-/-}$ total skin demonstrates that most HFA-GlcCer in mouse skin is present in SG, suggesting an important role for this sphingolipid in sebocytes. Although we could not purify SG from mouse skin, the absence of hydroxylated C20:0-GlcCer suggests that total HFA-GlcCer in FA2H-deficient SG is significantly reduced or may be absent. Currently, we do not know if also the concentration of total GlcCer is reduced or HFA-GlcCer is replaced by nonhydroxylated GlcCer in SG of *Fa2h*$^{-/-}$ mice.

In addition to its function in the synthesis of 2-hydroxylated fatty acids for HFA sphingolipid synthesis, FA2H is involved in formation of type II wax diesters. FA2H may directly be involved in production of wax diesters, by synthesizing 2-hydroxylated acyl-CoAs that are reduced to 1,2-diols by fatty acyl CoA reductases. Alternatively, HFA-GlcCer or other HFA sphingolipids may influence trafficking or activity of substrates or enzymes required for wax diester synthesis. At least the expression of these enzymes does not appear to be regulated by HFA sphingolipids, as the 2–3-fold up-regulation of *Far1*, *Far2*, and *Dgat1* in *Fa2h*$^{-/-}$ skin was in accordance with the SG enlargement. The presence of residual wax diesters in *Fa2h*$^{-/-}$ surface lipids may be due to the presence of a second hydroxylase enzyme (which may or may not be identical to the proposed hydroxylase enzyme in keratinocytes).

Delayed Hair Fiber Exit Because of Impaired SG Function—FA2H-deficient mice show some similarities to the *asebia* mouse mutant, which exhibits delayed hair fiber exit from follicles, caused by cornified cell plugs in the follicula ostia (38), possibly because of impaired sebum production. A similar, 2-day-delayed hair fiber exit was observed in mice deficient in

the lysosomal protease cathepsin L (48–50). Delayed emergence of the coat in *Ctsl*$^{-/-}$ mice was explained by defects in the desquamation of the inner root sheath at the level of the SG (50). We have not found evidence for impaired desquamation in *Fa2h*$^{-/-}$ mice, but the delay in fur appearance might be due to a block of the growing hair tip caused by the reduced fluidity of the sebum or the sebum plugs in the hair canal that apparently block the hair tip.

In wild-type mice, the new hair shaft is often formed before the old hair is shed in the exogen phase (1). Therefore, the normal repeated hair loss does not result in a cyclic alopecia. In the case of *Fa2h*$^{-/-}$ mice, loss of the old hair appears to start in telogen to early anagen, well before the new hair shaft is formed or exits the hair follicle, resulting in a cyclic alopecia. We propose that the premature hair loss is caused by accumulation of sebum in the infundibulum, which becomes dilated, although a premature induction of exogen cannot be excluded at present. The reduced amount of wax diesters together with the substantial increase in wax monoesters in *Fa2h*$^{-/-}$ mice may explain the significant increase in the melting point of the surface/sebum lipids.

As it has been shown for *asebia* mice, *Ctsl*$^{-/-}$ mice have a prolonged anagen phase/delayed catagen entry (48, 50). Similarly, preliminary data suggest a prolonged growing phase (morphogenesis and anagen) also in *Fa2h*$^{-/-}$ mice.[3] At least in case of *asebia* and *Fa2h*$^{-/-}$ mice, the signal causing this alteration of the hair cycle should originate in the SG. Because, in contrast to asebia mice, SG do not degenerate in *Fa2h*$^{-/-}$ mice, these mice may be useful to further explore SG-derived signals affecting the hair cycle.

FA2H Deficiency Causes Hyperproliferation of Sebocytes—EGF receptor/ErbB2 signaling appears to be essential for hair growth, and EGF signaling is turned off during anagen to catagen transition (51). Constitutive expression of EGF inhibits transition from anagen to catagen (51). The earliest change in gene expression in the back skin of *Fa2h*$^{-/-}$ mice was the strong up-regulation of *Epgn* in the basal layer of the SG and in some adjacent cells of the ORS. Epgn is a low affinity EGF receptor/ErbB1 ligand but has high mitogenic activity because of its weak ability to induce ErbB receptor degradation (52). Dahlhoff *et al.* (31) demonstrated a specific SG enlargement in *Epgn*-transgenic mice. Thus, *Epgn* up-regulation in *Fa2h*$^{-/-}$ mice is possibly responsible for the hyperproliferation of sebocytes. Because *Epgn* up-regulation was also found in adjacent cells outside the SG, which do not express *Fa2h* in wild type, we propose that FA2H or HFA sphingolipids do not directly control *Epgn* expression but most likely affect signaling pathways that possibly stimulate *Epgn* expression via a paracrine mechanism. The pathways causing *Epgn* up-regulation that are affected by HFA sphingolipids are not known. Although a number of studies clearly demonstrated that ceramides and several other "bioactive" sphingolipids play important roles in signal transduction (53), the role of the 2-hydroxyl modification of sphingolipids is largely unknown. Alderson and Hama (54) demonstrated that cAMP-dependent cell cycle exit of Schwannoma cells is impaired in the absence of FA2H, suggesting that HFA sphingolipids may negatively regulate the cell cycle. Inhibition of *Fa2h* expression has been shown to change mobility of "lipid raft" lipids and to alter GLUT4 localization and degradation (55). Thus, potentially HFA sphingolipids may also affect localization and/or the half-life of other (raft) membrane proteins and may thereby affect signal transduction. This, however, has not been demonstrated yet, and the signaling pathways directly affected by HFA sphingolipids are unknown at present.

[3] M. Meixner, H. Maier, and M. Eckhardt, unpublished observations.

REFERENCES

1. Schneider, M. R., Schmidt-Ullrich, R., and Paus, R. (2009) *Curr. Biol.* **19,** R132–R142
2. Milner, Y., Sudnik, J., Filippi, M., Kizoulis, M., Kashgarian, M., and Stenn, K. (2002) *J. Invest. Dermatol.* **119,** 639–644
3. Higgins, C. A., Westgate, G. E., and Jahoda, C. A. (2009) *J. Invest. Dermatol.* **129,** 2100–2108
4. Madison, K. C. (2003) *J. Invest. Dermatol.* **121,** 231–241
5. Smith, K. R., and Thiboutot, D. M. (2008) *J. Lipid Res.* **49,** 271–281
6. Schneider, M. R., and Paus, R. (2010) *Int. J. Biochem. Cell Biol.* **42,** 181–185
7. Nikkari, T. (1974) *J. Invest. Dermatol.* **62,** 257–267
8. Zheng, Y., Eilertsen, K. J., Ge, L., Zhang, L., Sundberg, J. P., Prouty, S. M., Stenn, K. S., and Parimoo, S. (1999) *Nat. Genet.* **23,** 268–270
9. Chen, H. C., Smith, S. J., Tow, B., Elias, P. M., and Farese, R. V., Jr. (2002) *J. Clin. Invest.* **109,** 175–181
10. Stenn, K. S., Zheng, Y., and Parimoo, S. (2008) *J. Invest. Dermatol.* **128,** 1576–1578
11. Holleran, W. M., Takagi, Y., and Uchida, Y. (2006) *FEBS. Lett.* **580,** 5456–5466
12. Alderson, N. L., Rembiesa, B. M., Walla, M. D., Bielawska, A., Bielawski, J., and Hama, H. (2004) *J. Biol. Chem.* **279,** 48562–48568
13. Eckhardt, M., Yaghootfam, A., Fewou, S. N., Zöller, I., and Gieselmann, V. (2005) *Biochem. J.* **388,** 245–254
14. Hama, H. (2010) *Biochim. Biophys. Acta* **1801,** 405–414
15. Uchida, Y., Hama, H., Alderson, N. L., Douangpanya, S., Wang, Y., Crumrine, D. A., Elias, P. M., and Holleran, W. M. (2007) *J. Biol. Chem.* **282,** 13211–13219
16. Zöller, I., Meixner, M., Hartmann, D., Büssow, H., Meyer, R., Gieselmann, V., and Eckhardt, M. (2008) *J. Neurosci.* **28,** 9741–9754
17. Ausubel, F. M., Brent, R., Kingston, R. E., Moore, D. D., Seidman, J. G., Smith, J. A., and Struhl, K. (2003) *Current Protocols in Molecular Biology,* John Wiley and Sons, New York
18. Fewou, S. N., Büssow, H., Schaeren-Wiemers, N., Vanier, M. T., Macklin, W. B., Gieselmann, V., and Eckhardt, M. (2005) *J. Neurochem.* **94,** 469–481
19. Paus, R., Müller-Röver, S., Van Der Veen, C., Maurer, M., Eichmüller, S., Ling, G., Hofmann, U., Foitzik, K., Mecklenburg, L., and Handjiski, B. (1999) *J. Invest. Dermatol.* **113,** 523–532
20. Doering, T., Brade, H., and Sandhoff, K. (2002) *J. Lipid Res.* **43,** 1727–1733
21. Jennemann, R., Sandhoff, R., Langbein, L., Kaden, S., Rothermel, U., Gallala, H., Sandhoff, K., Wiegandt, H., and Gröne, H. J. (2007) *J. Biol. Chem.* **282,** 3083–3094
22. Ponec, M., Weerheim, A., Lankhorst, P., and Wertz, P. (2003) *J. Invest. Dermatol.* **120,** 581–588
23. Wertz, P. W., and Downing, D. T. (1983) *J. Lipid Res.* **24,** 753–758
24. Wertz, P. W., and Downing, D. T. (1983) *J. Lipid Res.* **24,** 759–765
25. Fuchs, E. (2007) *Nature* **445,** 834–842
26. Riebeling, C., Allegood, J. C., Wang, E., Merrill, A. H., Jr., and Futerman, A. H. (2003) *J. Biol. Chem.* **278,** 43452–43459
27. Mizutani, Y., Kihara, A., and Igarashi, Y. (2005) *Biochem. J.* **390,** 263–271
28. Yen, C. L., Monetti, M., Burri, B. J., and Farese, R. V., Jr. (2005) *J. Lipid Res.* **46,** 1502–1511
29. Cheng, J. B., and Russell, D. W. (2004) *J. Biol. Chem.* **279,** 37789–37797
30. Gu, L. H., and Coulombe, P. A. (2008) *Am. J. Pathol.* **173,** 752–761
31. Dahlhoff, M., Müller, A. K., Wolf, E., Werner, S., and Schneider, M. R. (2010) *J. Invest. Dermatol.* **130,** 623–626

32. Zhang, L., Li, W. H., Anthonavage, M., and Eisinger, M. (2006) *Peptides* **27,** 413–420
33. Wille, J. J., and Kydonieus, A. (2003) *Skin Pharmacol. Appl. Skin Physiol.* **16,** 176–187
34. Georgel, P., Crozat, K., Lauth, X., Makrantonaki, E., Seltmann, H., Sovath, S., Hoebe, K., Du, X., Rutschmann, S., Jiang, Z., Bigby, T., Nizet, V., Zouboulis, C. C., and Beutler, B. (2005) *Infect. Immun.* **73,** 4512–4521
35. Thiele, J. J., Weber, S. U., and Packer, L. (1999) *J. Invest. Dermatol.* **113,** 1006–1010
36. Marques, M., Pei, Y., Southall, M. D., Johnston, J. M., Arai, H., Aoki, J., Inoue, T., Seltmann, H., Zouboulis, C. C., and Travers, J. B. (2002) *J. Invest. Dermatol.* **119,** 913–919
37. Gates, A. H., and Karasek, M. (1965) *Science* **148,** 1471–1473
38. Sundberg, J. P., Boggess, D., Sundberg, B. A., Eilertsen, K., Parimoo, S., Filippi, M., and Stenn, K. (2000) *Am. J. Pathol.* **156,** 2067–2075
39. Pennycuik, P. R., Raphael, K. A., Chapman, R. E., and Hardy, M. H. (1986) *Genet. Res.* **48,** 179–185
40. Selleri, S., Seltmann, H., Gariboldi, S., Shirai, Y. F., Balsari, A., Zouboulis, C. C., and Rumio, C. (2006) *J. Invest. Dermatol.* **126,** 711–720
41. Edvardson, S., Hama, H., Shaag, A., Gomori, J. M., Berger, I., Soffer, D., Korman, S. H., Taustein, I., Saada, A., and Elpeleg, O. (2008) *Am. J. Hum. Genet.* **83,** 643–648
42. Dick, K. J., Eckhardt, M., Paisán-Ruiz, C., Alshehhi, A. A., Proukakis, C., Sibtain, N. A., Maier, H., Sharifi, R., Patton, M. A., Bashir, W., Koul, R., Raeburn, S., Gieselmann, V., Houlden, H., and Crosby, A. H. (2010) *Hum. Mutat.* **31,** E1251–E1260
43. Watkins, P. A., Howard, A. E., and Mihalik, S. J. (1994) *Biochim. Biophys. Acta* **1214,** 288–294
44. Mukherji, M., Kershaw, N. J., Schofield, C. J., Wierzbicki, A. S., and Lloyd, M. D. (2002) *Chem. Biol.* **9,** 597–605
45. Foulon, V., Asselberghs, S., Geens, W., Mannaerts, G. P., Casteels, M., and Van Veldhoven, P. P. (2003) *J. Lipid Res.* **44,** 2349–2355
46. Baron, J. M., Wiederholt, T., Heise, R., Merk, H. F., and Bickers, D. R. (2008) *Curr. Med. Chem.* **15,** 2258–2264
47. Mizutani, Y., Kihara, A., Chiba, H., Tojo, H., and Igarashi, Y. (2008) *J. Lipid Res.* **49,** 2356–2364
48. Roth, W., Deussing, J., Botchkarev, V. A., Pauly-Evers, M., Saftig, P., Hafner, A., Schmidt, P., Schmahl, W., Scherer, J., Anton-Lamprecht, I., Von Figura, K., Paus, R., and Peters, C. (2000) *FASEB J.* **14,** 2075–2086
49. Tobin, D. J., Foitzik, K., Reinheckel, T., Mecklenburg, L., Botchkarev, V. A., Peters, C., and Paus, R. (2002) *Am. J. Pathol.* **160,** 1807–1821
50. Benavides, F., Starost, M. F., Flores, M., Gimenez-Conti, I. B., Guénet, J. L., and Conti, C. J. (2002) *Am. J. Pathol.* **161,** 693–703
51. Mak, K. K., and Chan, S. Y. (2003) *J. Biol. Chem.* **278,** 26120–26126
52. Kochupurakkal, B. S., Harari, D., Di-Segni, A., Maik-Rachline, G., Lyass, L., Gur, G., Kerber, G., Citri, A., Lavi, S., Eilam, R., Chalifa-Caspi, V., Eshhar, Z., Pikarsky, E., Pinkas-Kramarski, R., Bacus, S. S., and Yarden, Y. (2005) *J. Biol. Chem.* **280,** 8503–8512
53. Hannun, Y. A., and Obeid, L. M. (2008) *Nat. Rev. Mol. Cell Biol.* **9,** 139–150
54. Alderson, N. L., and Hama, H. (2009) *J. Lipid Res.* **50,** 1203–1208
55. Guo, L., Zhou, D., Pryse, K. M., Okunade, A. L., and Su, X. (2010) *J. Biol. Chem.* **285,** 25438–25447